Structural investigation of the *in vitro* transcript of the yeast tRNA^{phe} precursor by NMR and nuclease mapping

Kathleen B.Hall* and Jeffrey R.Sampson[1]
Department of Biochemistry and Molecular Biophysics, Washington University School of Medicine, Box 8231, 660 S.Euclid Ave, St Louis, MO 63110 and [1]Division of Biology, California Institute of Technology, Pasadena, CA 91125, USA

Received July 25, 1990; Revised and Accepted October 25, 1990

ABSTRACT

Both NMR and nuclease mapping have been used to probe the structure of an unmodified yeast tRNA^{phe} precursor synthesized in vitro by T7 RNA polymerase. A comparison of the NMR data of the precursor and of the mature tRNA transcript shows that the mature tRNA domain structure is similar in both molecules. In the tRNA precursor, the intron consists of a stem of at least four base-pairs, identified by NMR, and two single-stranded loops, identified by nuclease mapping. This is in agreement with the structure previously proposed for the native tRNA^{phe} precursor (1). However, our data also show the intron structure to be less stable than the mature tRNA domain, suggesting that the precursor may best be described as having two domains with a hinge at the junction of the anticodon and intron stems.

INTRODUCTION

Many tRNA genes in metazoans and archaebacteria encode intron sequences that are transcribed together with the tRNA sequence (2). Most of these tRNA introns are positioned within the anticodon loop, but at least one other is found in the variable loop (3). In S. cerevisiae precursors, the position of the intron beginning one nucleotide 3′ to the anticodon is invariant, and the introns are small, from 14 to 60 nucleotides. Either all or none of the yeast tRNA genes encoding an isoacceptor of a given tRNA will contain an intron (4). These intron-containing genes must of necessity be processed to produce the functional tRNA; the processing enzymes are therefore essential for cell viability.

Lee and Knapp (5) have proposed a consensus structure for yeast tRNA precursors based on structure-probing experiments. A central feature of this structure is the integrity of the tRNA portion, including secondary and tertiary interactions. The additional intron sequences form a new stem contiguous to the tRNA anticodon stem, base-pairing the anticodon nucleotides. The length of the intron stem and the size of the adjacent single-stranded loops vary with the specific intron sequence.

In S. cerevisiae, one endonuclease/ligase complex is responsible for processing all tRNA precursors (6,7). This has led to a model of the yeast endonuclease:precursor interaction which is guided by the conserved tRNA structural domain of the precursor (8). In this model of endonuclease recognition, the enzyme determines its cleavage sites after measuring an appropriate distance down the pre-tRNA structure from a contact point within the mature tRNA domain (the tRNA acting as a 'yardstick' (8)). Mutations in the mature tRNA domain most often influence processing (8−15), as can some base changes in the intron sequence (8,14,16).

In these experiments, we have studied the structure of the T7 RNA polymerase transcript of the S. cerevisiae tRNA^{phe} precursor. This in vitro transcript containing a 19-nucleotide intron has been shown to be a substrate for the yeast processing system (8). Using both NMR and nuclease mapping, we can ask detailed questions about the structure of the tRNA sequence, which can be directly compared to analogous structural information on the yeast tRNA^{phe} T7 transcript (17). In addition, the combination of NMR and nuclease mapping probes both the duplex regions of the intron structure and its single-stranded regions to provide a more detailed description of the precursor structure.

METHODS

The construction of the plasmid was described in Reyes and Abelson (8), and the use of T7 RNA polymerase to synthesize large amounts of transcript was described previously (17). The primary structure and the proposed secondary structure (1) of the precursor transcript is given in Figure 1, with the numbering convention indicated. As Reyes and Abelson have shown (8), this unmodified transcript is a substrate for the yeast processing enzymes.

Melting curves were measured on a Gilford 250 spectrophotometer, equipped with a thermal programmer. The heating rate was 1 °C/minute. The RNA concentration was 50 μg/mL in 5 mM $MgCl_2$, 100 mM NaCl, 10 mM $NaPO_4$, pH 7.0. The results of the first heating/cooling cycle were discarded, and samples were then heated and cooled twice to assure reproducibility.

* To whom correspondence should be addressed

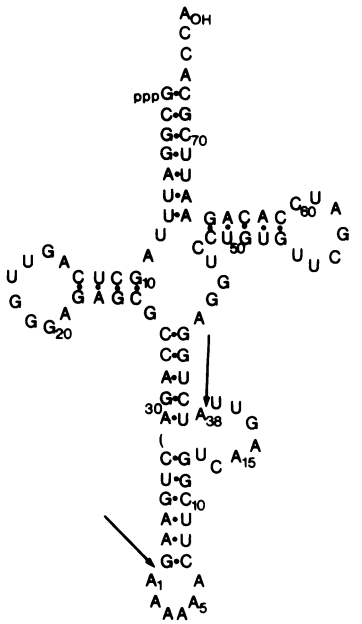

Figure 1. Primary structure and proposed secondary structure of the precursor transcript. Intron sequences are numbered from 1 to 19, and are referred to in the text as A_i1 etc. Splice sites are shown by arrows.

For NMR experiments, the transcript was dialyzed against 100 mM NaCl, 10 mM NaCacodylate pH 7 for 72 hours with several changes of dialysate. The final volume was adjusted to 200 μL with buffer and a final concentration of about 10% ^2H_2O to give a precursor concentration of 2 mM. $MgCl_2$ was added to a final concentration of 50 mM. Spectra were recorded using the 2-1-4 pulse for water suppression, with a spectral width typically 8kHz where the carrier was centered in the midst of the imino region. Recovery time was 500 msec. For NOE experiments, the pulse power and irradiation time were varied, and spectra were recorded in an interleaved mode with the off-resonance control. From 10,000 to 20,000 transients were averaged for the NOE experiments. The sequence of a base-paired helix can be determined from NOE experiments using the imino protons, as first described by Roy and Redfield for yeast $tRNA^{phe}$ (18). The efficiency of magnetization transfer between imino protons on adjacent base-pairs is often poor, however, as it is dependent on the distance between bases and influenced by the stability of the helix. NOE efficiencies of 1−5% dictate the number of transients. Saturation recovery experiments were done by saturating the entire imino proton region using either CHIRP or WALTZ sequences, then following the recovery of the magnetization at variable times. NMR experiments used the 500 MHz spectrometer at Brandeis University in the laboratory of Prof. A.G. Redfield.

For nuclease mapping, the transcript was 3′ end-labelled using (5′^{32}P)pCp and T4 RNA ligase as described (19), and purified by denaturing gel electrophoresis. Purification was not sufficiently precise to resolve the heterogeneous products resulting from 3′ end addition by T7 RNA polymerase. After recovery from the gel, the RNA was resuspended in distilled water. Each nuclease digestion reaction contained approximately 25 cps of ^{32}P-labelled RNA and 10 μgram of carrier yeast tRNA. Prior to addition of enzyme, the tRNA mixture was heated to 65 °C for 10 minutes in the appropriate buffer and allowed to slowly cool to room temperature. The enzyme concentrations were adjusted by titration to give only primary cleavages. The buffer used for nuclease T1 digestion included 200 mM NaCl, 10 mM Tris, pH 7; for nuclease U2: 200 mM NaCl, 25 mM NaAcetate pH 5.5; the U2 buffer plus 1 mM $ZnSO_4$ was used for nuclease S1 digestions. All buffers contained either 5 mM $MgCl_2$ or 1 mM EDTA. Marker lanes were obtained by digestion with 100X excess of enzyme; this method produces different digestion patterns in conditions ± $MgCl_2$. Reactions were stopped by the addition of 200 μL of 0.5 mg/ml proteinase K in 150 mM NaCl, 12 mM EDTA, 100 mM Tris pH 7.5, and 1% SDS, and incubated at 45 °C for 15 minutes, followed by phenol extraction and ethanol precipitation. Reaction temperatures are indicated in the Figures. After final precipitation, the RNA was resuspended in formamide solution, heated to 90 °C, and electrophoresed on 12% polyacrylamide, 8 M urea gels.

RESULTS

NMR Analysis

For the structural comparison of the precursor with the tRNA, the precursor NMR spectra were taken in 50 mM added $MgCl_2$, while the tRNA data were aquired in 5 mM free Mg^{++}. The difference in the NMR spectra of the tRNA transcript at these two Mg^{++} concentrations is minimal, and was discussed in detail previously (17). Briefly, the significant features are a) a shift in the position of the resonance assigned to the tertiary base-pair U54A58 and b) the disappearance in 5 mM free Mg^{++} of several broad resonances near 11 ppm that were present in 50 mM total $MgCl_2$. In 50 mM added $MgCl_2$, the U54A58 resonance is found in a single peak at 13.6 ppm; in 5 mM free Mg^{++} it is found in a composite peak at 13.77 ppm. Additional free Mg^{++} (at least to 10 mM) does not alter the spectrum. The spectrum of the precursor in 50 mM added $MgCl_2$ resembles that of the tRNA in 5 mM free Mg^{++} in that first, the imino proton resonance from U54A58 is already part of the composite peak at 13.77 ppm, and second, there are no imino proton resonances at 11 ppm. This similarity, and the correspondence in chemical shift of the other resonances, are evidence that the two Mg^{++} conditions have produced similar tRNA conformations in the two molecules.

The imino proton spectrum of the tRNA precursor transcript in 50 mM added $MgCl_2$ closely resembles that of the $tRNA^{phe}$ transcript in 5 mM free Mg^{++} (Figure 2) with the obvious addition of four distinct resonances and three apparent increases in peak intensity. These changes are seen clearly in a difference plot, shown in Figure 2, in which the spectrum of the tRNA transcript has been subtracted from that of the precursor. As indicated, there are four new resonances in the precursor spectrum including peak b at 14.24 ppm, peak l at 11.95 ppm, peak n at 11.52 ppm, and peak p at 10.68 ppm (at 30 °C). Additional resonances are present at 13.77 ppm (c3) and at 12.4 ppm (j), which overlap with existing resonances, and there is possibly a shift of a resonance at peaks g and h (12.97 and 12.8 ppm respectively). There is also additional intensity in peak q at 10.43 ppm.

A comparison of the chemical shifts of the imino proton resonances of the precursor and the $tRNA^{phe}$ transcript is shown in Table I. Both the chemical shifts, and more significantly, the NOE patterns of the conserved resonances (data not shown) are nearly identical in the two spectra. The assignment of the tRNA resonances has been described (17) and can be confidently applied to the spectrum of the precursor. Those assignments are also indicated in Table I. The identification of the tertiary interactions

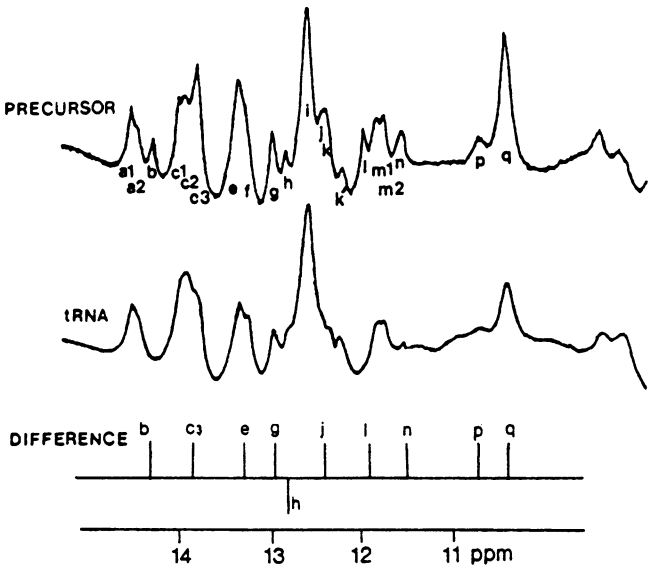

Figure 2. Imino proton NMR spectra of the precursor transcript and the normal $tRNA^{phe}$ transcript, at 30 °C in 90%H_2O:10%D_2O. The precursor transcript is in 50 mM total $MgCl_2$ and the tRNA in 5 mM free Mg^{++}, each with 100 mM NaCl, 10 mM NaCacodylate, pH 7. RNA is 2 mM. Spectra were taken on a 500 MHz spectrometer using the 2-1-4 sequence for water suppression. The difference plot (precursor−tRNA) is obtained by overlaying the two spectra after normalizing for the intensity of peak a1 and manually subtracting the tRNA spectrum from that of the precursor. The bar graph representation is for ease of visualization, and is not meant to indicate relative intensities. The positive bars indicate a new resonance (intensity) at that chemical shift in spectrum of the precursor, while negative bars indicate loss of a resonance (intensity) at that chemical shift in the precursor.

characteristic of the folded cloverleaf is especially important in establishing that the tRNA conformation is normal, even with the addition of the intron.

Identification of the base-pair type (AU, CG, or GU) of the precursor-specific resonances relied on NOE experiments and chemical shift arguments. Peaks b and c3 show strong sharp NOEs to the aromatic region, at 7.54 ppm and 7.22 ppm respectively (at 30 °C), thus identifying them as AU imino protons on the basis of their NOEs to AH2 protons. On the basis of chemical shift, peak l at 11.95 ppm is identified as a GC imino proton resonance. Peak n shows an NOE to and from peak q, indicating that there is a another precursor-specific new resonance in that rather broad peak, in agreement with the difference spectrum. In the spectra of both the tRNA and the precursor transcripts, peak q gives a strong NOE (30%) to peak m1, providing an unambiguous identification of the two imino protons of G4U69 in the acceptor stem. The chemical shift of peak q is far upfield for a GC imino proton, and so by analogy suggests that the q-to-n NOE in the precursor is also indicative of a GU base pair. No NOEs are observed to or from peak p, the weak resonance at 10.68 ppm. Resonances at this upfield chemical shift have been tentatively assigned to imino protons of bases in loops where they are protected from solvent exchange (20,21) and it is not unreasonable that this is the origin of peak p here. No new NOEs are seen to or from the resonance at 12.4 ppm identified in the difference spectrum, but in this crowded region of the spectrum it is very difficult to obtain unambiguous data.

The relative position of these new base-pairs in the precursor structure was established by observing the patterns of interbase-pair NOEs (18). Several NOE difference spectra used for assignments are shown in Figure 3. Similar experiments were

Table I. Imino Proton Chemical Shifts and Assignments of Precursor and $tRNA^{phe}$ Transcripts

Peak[a]	Chemical Shift(ppm)[b] Pre-phe	$tRNA^{phe}$	Assignment[c,d]
a1	14.48	14.48	A: U6A67
a2	14.41	14.41	3: U8A14
b	14.24		I: A36U_i8
c1	13.98	13.98	A: A5U68
c2	13.9	13.87	D: A23U12
c3	13.77	13.79	3: U54A58
			T: U50A64
			I: A35U_i9
e	13.29	13.31	A: U7A66
			T: U52A62
f	13.23	13.21	AC: A29U41
g	12.97	12.96	D: G22C13
h	12.8	12.8	D: G24C11[t]
i	12.57	12.57	A: C2G71
			T: C49G65 G53C61
			T: C25G10[t]
			AC: C28G42
j	12.41	12.36	T: G51C63
k	12.36	12.36	A: G3C70
k'	12.20	12.24	3: G15C48
l	11.95		I: G34C_i10
m1	11.84	11.82	A: G4U69
m2	11.72	11.76	3: G18U55
n	11.52		I: U33G_i11
p	10.68		
q	10.43	10.43	A: G4U69
			I: U33G_i11

[a] Peak positions at 30°C in 50 mM $MgCl_2$ for precursor and in 5 mM free Mg^{++} for tRNA. See Figure 1.
[b] Chemical shifts are relative to H_2O at 4.8 ppm.
[c] A: acceptor stem; T: T-stem; D: D-stem; AC: anticodon stem; I: intron stem; 3: tertiary interaction. For assignment logic of the tRNA portion, see Hall et al. (17).
[d] N_i indicate intron sequences.
[t] Tentative assignment.

recorded at various temperatures and irradiation times. Imino-imino proton NOEs are often difficult to observe, since they are weak and the lines are broad. Few imino-imino cross-peaks are observed in two-dimensional experiments (NOESY) of these RNAs, so these experiments were not used for the precursor molecule. Nevertheless, reciprocal 1D NOEs are observed between peaks n and l, between l and c3, and between c3 and b, thus indicating that the new resonances in the precursor spectrum arise from base-pairs comprising a new stacked stem. The sequence of this helix can be identified as GU,GC,AU,AU (nq,l,c3,b), or alternatively AU,AU,GC,GU, since no conclusion can be made about the orientation (5′ or 3′) of the base pairs.

Nuclease Mapping

Previous structure-probing experiments of the partially modified native $tRNA^{phe}$ precursor reported by Swerdlow and Guthrie (1) indicated that this molecule conforms to the consensus structure proposed by Lee and Knapp (5). These data thus provide a reference for the nuclease-mapping of the transcript precursor, and allow a comparison of the properties of the molecule with and without modified bases. In addition, nuclease mapping can more quickly probe for conformational changes as a function of solution conditions (e.g. ± Mg^{++}) than can analogous NMR experiments.

Probing the precursor structure in 5 mM added $MgCl_2$ with single-strand specific enzymes indicates that two regions near and including the intron sequence are single-stranded: from A_i1

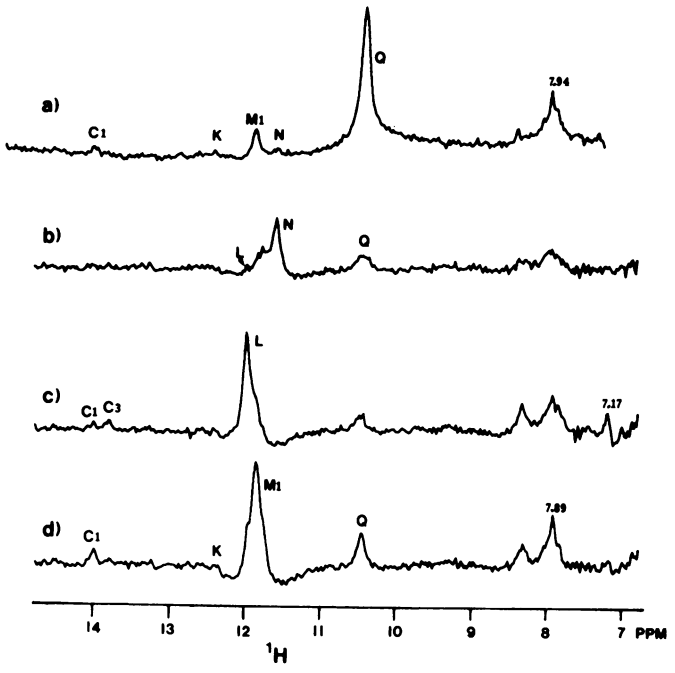

Figure 3. NOE difference spectra of the precursor. a) Irradiating peak q at 30 °C for 500 msec shows NOEs to peaks m1, k, and c1 (7.94 ppm AH2) assigned to the acceptor stem, and to peak n, unique to the precursor. b) Irradiating peak n at 25 °C shows NOEs to peak q and a weak NOE to peak l. c) Irradiating peak l at 25 °C shows an NOE to peak c3 (7.17 ppm AH2) from the precursor and to peak c1 which is spillover from peak m1. Other experiments show an l-to-n NOE. d) Irradiating peak m1 at 25 °C to illustrate the spill-over effects seen in 1c). In experiments b)–d) irradiation was for 300 msec.

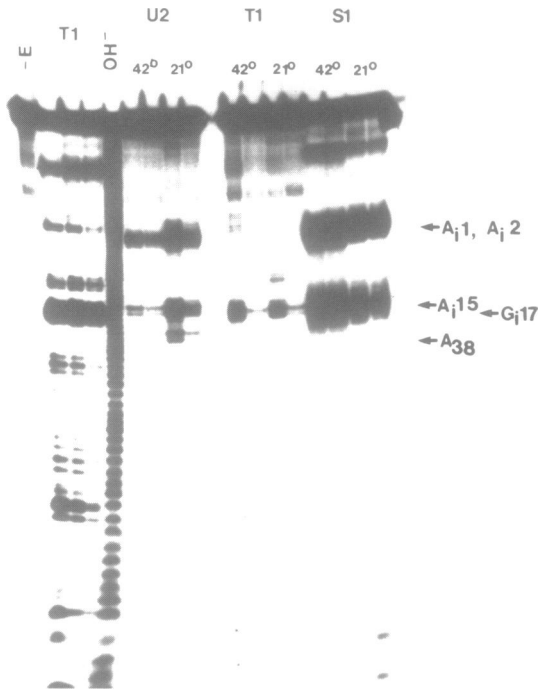

Figure 4. Nuclease mapping the precursor transcript in 5 mM $MgCl_2$. The doublets that appear in the figures are the result of heterogeneity at the 3′ end produced by T7 RNA polymerase. Conditions for enzymatic digestion as described in Methods. From the left: -E: no enzyme added; T1: extensive nuclease T1 digestion to provide markers; OH^-: base hydrolysis ladder; U2: nuclease U2 digestion at 42 °C for 10 and 5 minutes, and at 21 °C for 10 and 5 minutes; T1: nuclease T1 digestion at 42 °C and 21 °C for 10 and 5 minutes; S1: nuclease S1 digestion at 42 °C and 21 °C for 10 and 5 minutes. Primary cleavage sites are labelled.

to A_i4, and A_i15 and G_i17 extending through A38 (see Figure 4). Primary cleavages are seen at A_i1, A_i2, A_i15, A_i16, G_i17, and A38. Secondary sites are observed upon longer exposure of the autoradiogram (data not shown). Significantly, other regions of the tRNA sequence are not readily nuclease accessible. Nuclease accessibility is not altered by increasing the temperature from 21 °C to 42 °C in these experiments.

Intron Stability

The melting curve of the precursor transcript shown in Figure 5 does not have the sharp cooperative transition of the tRNA transcript, but shows an additional broader transition. Subtracting the melting profile of the tRNA from that of the precursor shows a broad peak centered at 64 °C, shown in Figure 5, which probably originates in the intron. In support of this interpretation, saturation recovery experiments at 26 °C show that the base-pairs of the intron (using peaks b and l as representative since they are cleanly separated and at opposite ends of the intron stem) and the tRNA (using peak a1 as representative) have nearly identical T_1 values (spin lattice relaxation rate). When the experiment is repeated at 34 °C, the T_1 of peaks b and l are 2–3 times that of peak a1, and at 45 °C, the spin lattice relaxation rate of intron peak b is about 5 times faster than the rate of the tRNA peak a1. These experiments, which effectively measure the accessibility of the imino proton to solvent, indicate that the base-pairs of the intron structure are not as stable as those of the tRNA at higher temperature, suggesting that the intron structure will melt before the tRNA portion.

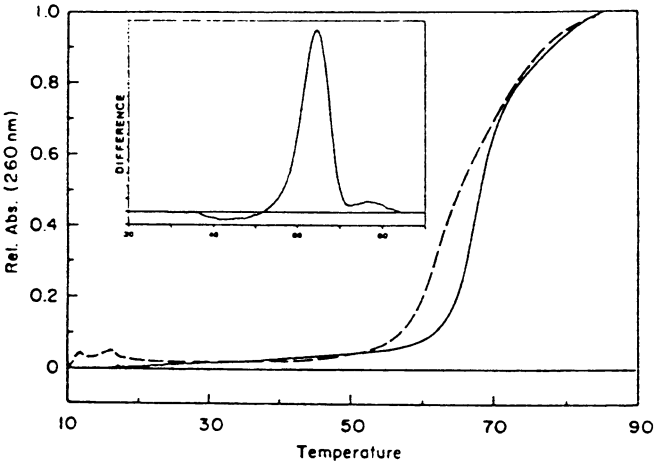

Figure 5. Thermal melting profile of the precursor (– –) and the $tRNA^{phe}$ transcript (–). A difference spectrum (inset) shows an additional transition in the precursor. Conditions were 5 mM $MgCl_2$, 100 mM NaCl, and 10 mM $NaPO_4$, pH 7.0.

Alternative conformations

NMR Results

Because the tRNA transcript can undergo a Mg^{++}-dependent conformational change (17,22) we looked at the effect of Mg^{++} on the conformation of the precursor. The imino proton NMR spectrum of the precursor is compared to that of the tRNA transcript in the absence of Mg^{++} in Figure 6. The difference

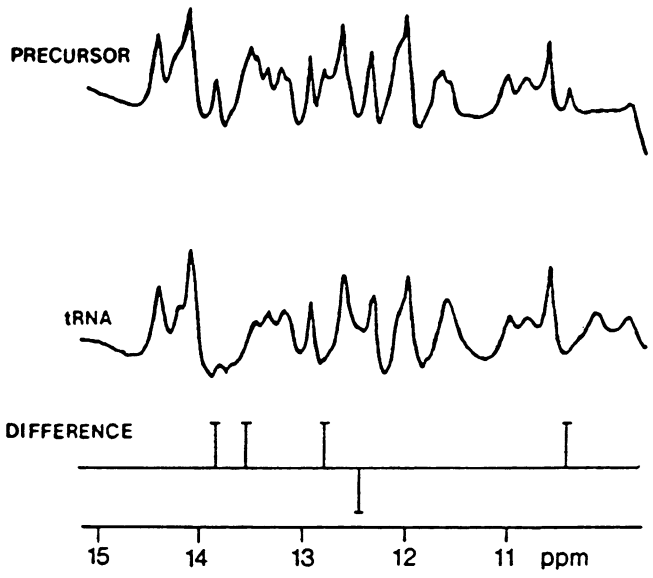

Figure 6. Imino proton NMR spectra of the precursor and tRNA^{phe} transcripts in the absence of $MgCl_2$, with 100 mM NaCl, 10 mM NaCacodylate, pH 7, at 30 °C. As per Figure 2, the difference plot was obtained by a manual subtraction of the tRNA spectrum from that of the precursor after normalizing the peak intensity of peak a (assigned to an AU pair in the acceptor stem). Positive bars indicate a new resonance in the precursor spectrum at that chemical shift, negative bars indicate absence of a peak in the precursor spectrum.

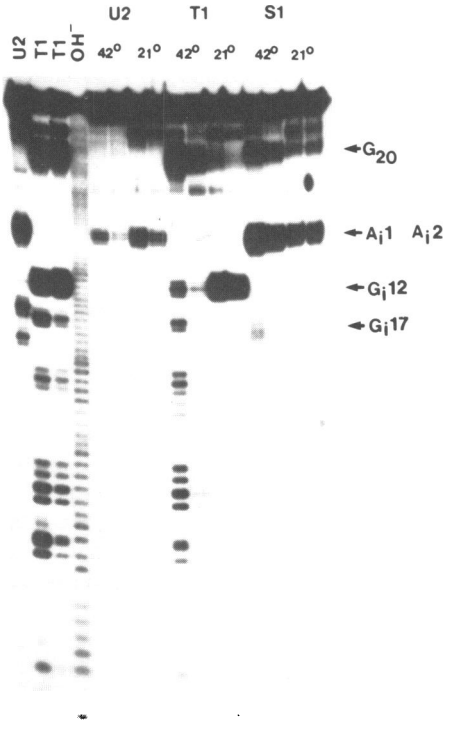

Figure 7. Nuclease cleavage of the precursor in the absence of $MgCl_2$ (with 1 mM EDTA). Three lanes on the left labelled U2 and T1 are more extensive digestions of the precursor to provide markers. Other lanes are per Figure 4.

plot shows that there are apparently only four additions to the precursor spectrum: two in the AU region, one on the CG region and one far upfield. At 12.4 ppm, in the GC region, there is

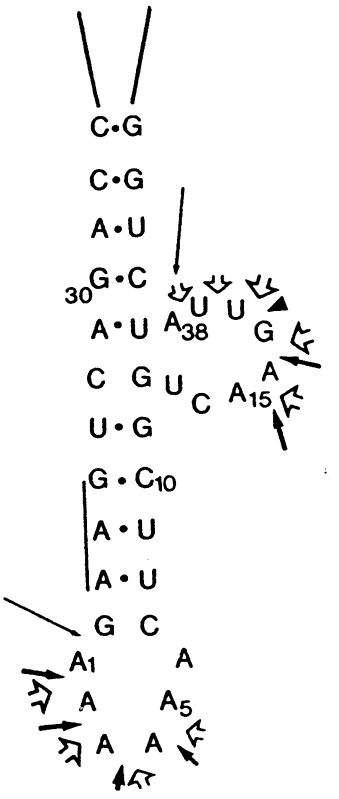

Figure 8. Structure of the precursor intron in the presence of Mg^{++}. Underlined nucleotides GAA indicate the yeast tRNA^{phe} anticodon sequence. The two end-terminal base-pairs of the intron stem are shown stacked but not paired, for these base-pairs are not identified by NMR. Splice sites are labelled with thin long arrows. Nuclease sites are indicated: solid tailed arrows, U2; solid arrow, T1; open arrow, S1. Larger, darker arrows with longer tails indicate primary cleavages; other arrows show secondary cleavage sites identified in longer exposure of the original autoradiograms.

an apparent loss of a resonance in the spectrum of the precursor. Little of the tRNA spectrum was assigned in these conditions, with the exception of the base-pairs of the acceptor stem (17). In the spectrum of the precursor under the conditions of no Mg^{++}, the imino proton resonances of the acceptor stem were found at their analogous tRNA chemical shifts, and again assigned through their NOE patterns (data not shown), but no further assignments were done.

Nuclease mapping results

Nuclease cleavage patterns provided unambiguous evidence that the intron conformation alters in the absence of Mg^{++} (see Figure 7). While nucleotides A_i1 to A_i4 remain single-stranded, G_i12 becomes the primary T1 cleavage site; now G_i17 and A_i16 are no longer nuclease accessible. Cleavage of the tRNA is also seen at G18, G19, and G20 in the D-loop in these conditions, indicating that the tertiary interactions have been destabilized or disrupted. However, no new cleavage sites appear in what would normally be stem regions of the tRNA, indicating that there has been no rearrangment of the normal cloverleaf structure. Addition of 5 mM spermidine restores cleavage at G_i17 and to some extend at A_i16, but does not decrease G_i12 accessibility (data not shown), suggesting that both conformations are present.

Such conformational flexibility cannot be wholely attributed to the absence of modified bases in the transcript, for the native precursor also lacks modified bases in the anticodon stem and loop region where they might be expected to exert the greatest

effect on the stability of the adjacent structures (23). The ability of the intron sequence to form alternative conformations as a function of counterion concentrations may have biological implications if one structure is the preferred substrate for the endonuclease.

DISCUSSION

Consensus Structure

Combining the results from NMR and nuclease mapping with the primary structure of the precursor produces the structure of the intron as indicated in Figure 8. Here, the nucleotides of the normal anticodon loop are base-paired in a stem, with two new single-stranded loops, one at the end of the stem, and one between the normal anticodon stem and the start of the new intron stem. This structure is nearly identical to that proposed by Swerdlow and Guthrie (1) on the basis of their nuclease mapping experiments of the native $tRNA^{phe}$ precursor, and shows that the in vitro transcript can adopt the same structure as the partially modified native precursor. Calculations of the free energy (24) of the structure including the anticodon stem and the intron sequences give a favorable $\Delta G = -4.3$ kcal/mol.

An important result from the NMR data is that the structure of the tRNA in the precursor is nearly identical to that of the normal tRNA, with the possible exception of the anticodon stem (which has not been completely assigned in NMR experiments). This result was expected based on previous structure-probing of native precursors (1,5), but the NMR data show directly that normal tRNA secondary and tertiary interactions are present in the precursor.

Deviations from consensus?

Several features of the intron structure are unexpected, however, and may have implications for biological activity. The intron stem appears to be shorter than anticipated, for while the proposed intron stem contains six base-pairs (1), only four can be found by NMR; the two end-terminal GC pairs are not identified in NOE experiments. It is very likely that the 3′ terminal $G37C_i7$ pair is present, since the two contiguous AU pairs can be readily identified in the NMR spectrum by NOE experiments, and neither A36 nor G37 is a site of single-strand specific nuclease cleavage. If $G37C_i7$ were absent, the terminal $A36U_i8$ pair would be more labile, and so decrease the intensity of its imino proton resonance and make the NOEs more difficult to observe. At the 5′ end of the intron stem, there is some suggestion of an NOE from $U33G_i11$ to a resonance in peak e, indicative of an additional stacked base-pair, but the evidence is not strong enough to be certain. The relatively low intensity, temperature sensitivity, and broad line-width of the imino proton resonance assigned to $U33G_i11$ indicate that this base-pair is not stable, which in turn suggests that the postulated $C32G_i12$ on its 5′ side may be only transiently associated. If the terminal base-pairs of the stem, $C32G_i12$ and $G37C_i7$, are not stably hydrogen-bonded, then their imino protons would exchange much more rapidly with water, and not be visible in the spectrum.

On the basis of the NOE patterns observed, the intron helix does not appear to be coaxial with the anticodon helix. If the anticodon helix were stacked on the intron helix, the base-pairs at the junction would be expected to be sufficiently stable to be observed in the NMR spectrum, and hopefully there would be an NOE observed between them. Stabilizing the anticodon stem should then allow more of its resonances to be identified and assigned, but this was not observed. Making structural conclusions based solely on the absence of an NOE is never wise, as in this case these two helices may actually be coaxial but the distance between their two terminal base-pairs may exceed the limit for observable NOE transfer. However, the absence of any NOE linking the two helices, together with the lower melting temperature of the intron sequences and the shorter T_1 relaxation times of the imino proton resonances of the intron helix suggest that the intron helix and the anticodon stem are not coaxially stacked.

Possible structural contributions to processing

The integrity of the tRNA structure in the precursor is a critical feature of the model for endonuclease cleavage proposed by Reyes and Abelson (8). Both our data, and those of Swerdlow and Guthrie (1) indicate that the tRNA portion of the precursor is intact. Mutations that affect this structure would be expected to affect processing, as indeed some do (8,13,14).

The role of the intron structure to the process of intron excision is unclear (11,13,16,25,26). While a common structure can be found for tRNA introns of S. cerevisiae (5), the analogous introns of S. pombe appear to be unstructured yet are acceptable substrates for the S. cerevisiae enzymes (14,27). An unstructured polyU(G) sequence in place of the normal S. cerevisiae $tRNA^{phe}$ intron was also an acceptable substrate (8), showing that the endonuclease can locate the correct cleavage sites in unstructured introns. Yet other results suggest that the endonuclease is apparently unable to disrupt duplex RNA to facilitate cleavage (26,28). Our results, which suggest that the yeast $tRNA^{phe}$ intron is not rigidly appended to the tRNA structure, would then support the idea that some conformational flexibility of the precursor contributes to processing. It is possible that the large single-stranded loop between the anticodon and intron helices contributes to efficient processing by defining and destabilizing the intron sequences of the precursor.

SUMMARY

Lee and Knapp (5) have proposed a consensus structure for yeast tRNA precursors, which appears from our experiments to be mostly correct for the $tRNA^{phe}$ transcript. In agreement with their model, we have shown that the tRNA portion of the molecule adopts essentially the same structure both with and without the intron. However, the consensus model predicts coaxial stacking of the anticodon helix and the intron helix, and for this precursor, that is not observed. Rather, the intron structure seems distinct from the adjacent tRNA, such that it may be more correct to think of a hinge between the two helices that defines two dynamically distinct domains of the precursor.

ACKNOWLEDGEMENTS

We thank Al Redfield for the generous use of his spectrometer, Olke Uhlenbeck and the members of his lab for their hospitality and generosity, and John Abelson for his interest and comments. Chris Greer and Calvin Ho provided helpful criticism of the manuscript, and we thank C.Greer and Gayle Knapp for thoughtful discussions. This work was supported in part by the National Institutes of Health GM20168 (A.G.Redfield), GM37552 (O.C.Uhlenbeck), and the Lucille P.Markey Charitable Trust #88-30 (K.B.H.).

REFERENCES

1. Swerdlow, H. and Guthrie, C. (1984) J. Biol. Chem. **259**, 5197–5207.
2. Culbertson, M.R. and Winey, A. (1989) Yeast **5**, 405–427.
3. Kjems, J., Leffers, H., Olesen, T. and Garrett, R.A. (1989) J. Biol. Chem. **264**, 17834–17837.
4. Ogden, R.C., Lee, M.C., and Knapp, G. (1984) Nucleic Acids Res **12**, 9367–9382.
5. Lee, M.C. and Knapp, G. (1985) J. Biol. Chem. **260**, 3108–3115.
6. Peebles, C.L., Gegenheimer, P. and Abelson, J. (1983) Cell **32**, 525–536.
7. Phizicky, E.M., Schwartz, R.C., and Abelson, J. (1986) J. Biol. Chem. **261**, 2978–2986.
8. Reyes, V.M. and Abelson, J. (1988) Cell **55**, 719–730.
9. Nishikura, K., Kurjan, J., Hall, B.D., and DeRobertis, E.M. (1982) EMBO J. **1**, 263–268.
10. Gandini-Attardi, D., Margarit, I., and Tocchini-Valentini, G., (1985) EMBO J. **4**, 3289–3297.
11. Strobel, M.C. and Abelson, J. (1986) Mol. Cell. Biol. **6**, 2663–2673.
12. Strobel, M.C. and Abelson, J. (1986) Mol. Cell. Biol. **6**, 2674–2683.
13. Mattoccia, E., Baldi, I.M., Gandini-Attardi, D., Ciafre, S., and Tocchini-Valentini, G. (1988) Cell **55**, 731–738.
14. Willis, I., Hottinger, H., Pearson, D., Chisholm, V., Leupold, U., and Soll, D. (1984) EMBO J. **3**, 1573–1580.
15. Colby, D., Leboy, P.S., and Guthrie, C. (1981) Proc. Natl. Acad. Sci. U.S.A. **78**, 415–419.
16. Greer, C.L., Soll, D. and Willis, I., (1987) Mol. Cell. Biol. **7**, 76–84.
17. Hall, K.B., Sampson, J.R., Uhlenbeck, O.C. and Redfield, A.G. (1989) Biochem **28**, 5794–5801.
18. Roy, S. and Redfield, A.G. (1981) Nucleic Acids Res. **9**, 7073–7083.
19. Bruce, A.G. and Uhlenbeck, O.C. (1978) Nucleic Acids Res. **4**; 2527–2534.
20. Haasnoot, C.A.G., de Bruin, S.H., Berendsen, R.G., Janssen, H.G.J.M., Binnendijk, T.I.J., Hilbers, C.W., van der Marel, G.A., and van Boom, J.H. (1983) J. Biomol. Stereodyn. **1**, 115–129.
21. Clore, G.M., Gronenberg, A.M., Piper, E.A., McLaughlin, L.W., Greaser, E., and van Boom, J.H. (1984) Biochem J. **221**, 737–750.
22. Hall, K.B. and Sampson, J.R. (1990) J. Biomol. Stereodyn. Structure and Methods Vol. 3, *DNA and RNA* p. 297–307.
23. Knapp, G., Becknamm, J.S., Johnson, P.F., Fuhrman, S.A. and Abelson, J. (1978) Cell **14**, 221–236.
24. Freier, S.M., Kiersek, J.A., Jaeger, J.A., Sujimoto, N., Caruthers, M.H., Neilson, T., and Turner, D.H. (1986) Proc. Natl. Acad. Sci. U.S.A. **83**, 9373–9377.
25. Raymond, G. and Johnson, J.D. (1983) Nucleic Acids Res. **11**, 5969–5988.
26. Szekeley, E., Belford, H.G. and Greer, C.L. (1988) J Biol Chem **263**, 13839–13847.
27. Pearson,D., Willis, I., Hottinger, H., Bell, J., Kumar,A., Leupold, U., and Soll, D. (1985) Mol. Cell Biol. **5**, 808–815.
28. Baldi, M.I., Mattoccia, E., Ciafre, S., Gandini Attardi, D., Tocchini-Valentini,G. (1986) Cell **47**, 965–971.